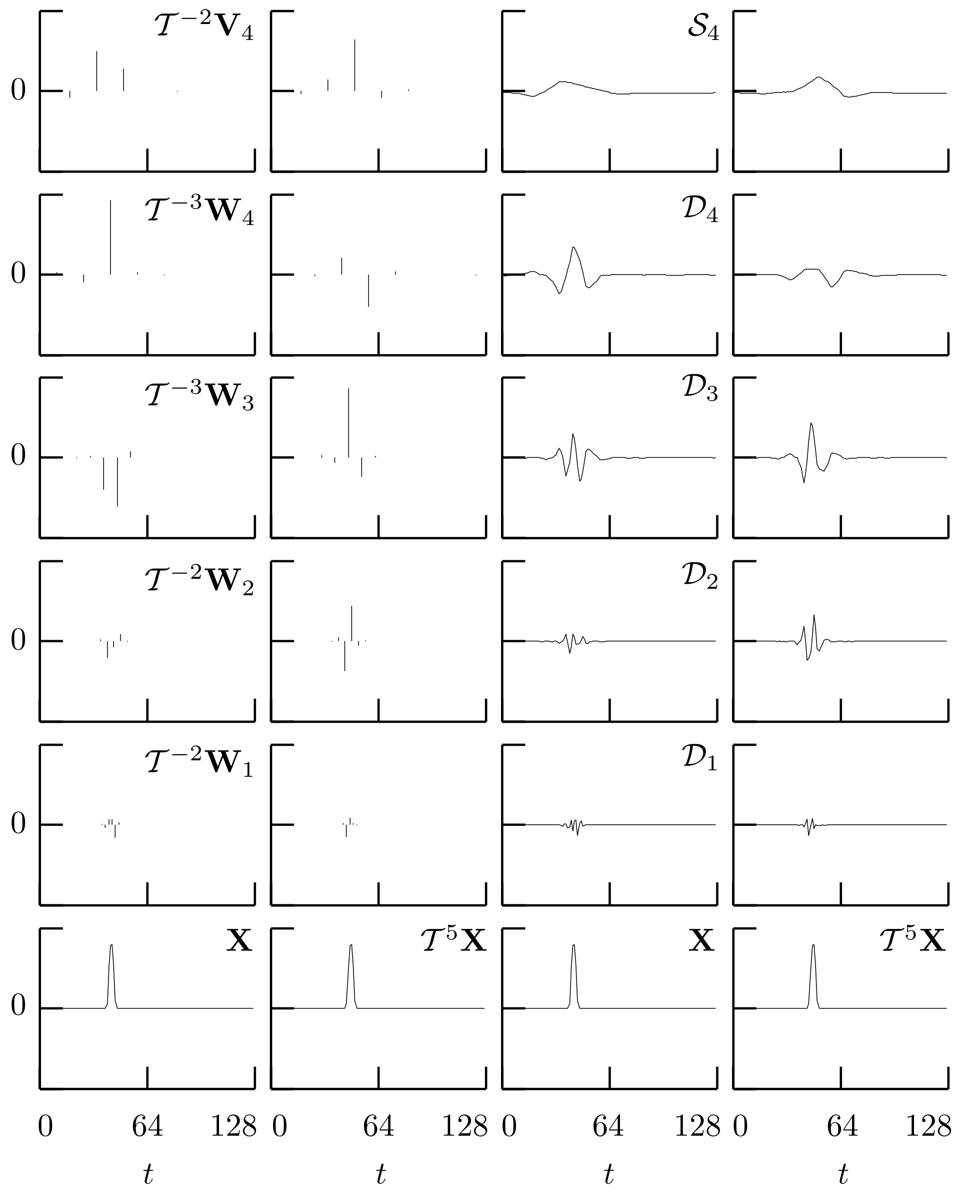

Figure 161. LA(8) DWTs of level $J_0 = 4$ (top five rows, first two columns) and corresponding multiresolution analyses (last two columns) for a time series $\mathbf{X}$ and its circularly shift $\mathcal{T}^5\mathbf{X}$ (bottom row of plots). A comparison of the first and second columns shows that circularly shifting a time series can yield substantial changes in its DWT; likewise, the third and fourth columns indicate the same is true for the corresponding MRAs. This figure should be compared with Figure 181, which uses the MODWT in place of the DWT.

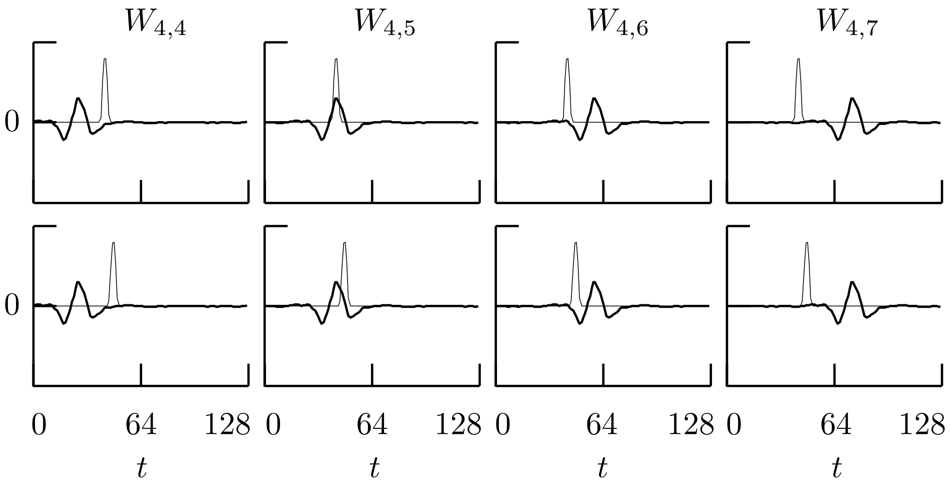

Figure 162. Level $J_0 = 4$ basis vectors used in the LA(8) DWT to produce the wavelet coefficients $W_{4,j}$, $j = 4, \ldots, 7$ (thick curves, respectively, from left to right in both rows of plots), along with a 'bump' time series $\mathbf{X}$ (thin curves in top row of plots) and $\mathcal{T}^5\mathbf{X}$ (thin curves, bottom row). The inner product between a plotted basis vector and a time series yields the wavelet coefficient labeled at the top of the figure.

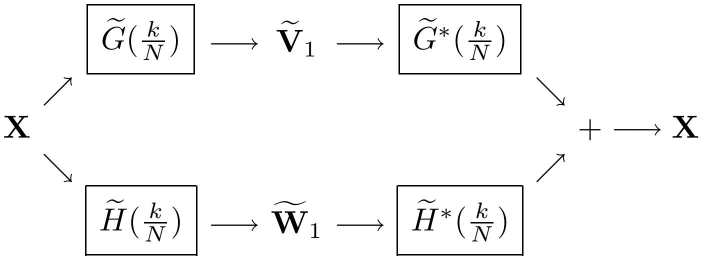

Figure 169. Flow diagram illustrating analysis of $\mathbf{X}$ into the MODWT wavelet and scaling coefficients $\widetilde{\mathbf{W}}_1$ and $\widetilde{\mathbf{V}}_1$ of first level, followed by the synthesis of $\mathbf{X}$ from $\widetilde{\mathbf{W}}_1$ and $\widetilde{\mathbf{V}}_1$.

$$\begin{tikzcd}
 & \boxed{\widetilde{G}(2^{j-1}\frac{k}{N})} \arrow[r] & \widetilde{\mathbf{V}}_j \arrow[r] & \boxed{\widetilde{G}^*(2^{j-1}\frac{k}{N})} \arrow[dr] & & \\
\widetilde{\mathbf{V}}_{j-1} \arrow[ur] \arrow[dr] & & & & + \arrow[r] & \widetilde{\mathbf{V}}_{j-1} \\
 & \boxed{\widetilde{H}(2^{j-1}\frac{k}{N})} \arrow[r] & \widetilde{\mathbf{W}}_j \arrow[r] & \boxed{\widetilde{H}^*(2^{j-1}\frac{k}{N})} \arrow[ur] & &
\end{tikzcd}$$

Figure 175. Flow diagram illustrating analysis of $\widetilde{\mathbf{V}}_{j-1}$ into $\widetilde{\mathbf{W}}_j$ and $\widetilde{\mathbf{V}}_j$, followed by the synthesis of $\widetilde{\mathbf{V}}_{j-1}$ from $\widetilde{\mathbf{W}}_j$ and $\widetilde{\mathbf{V}}_j$.

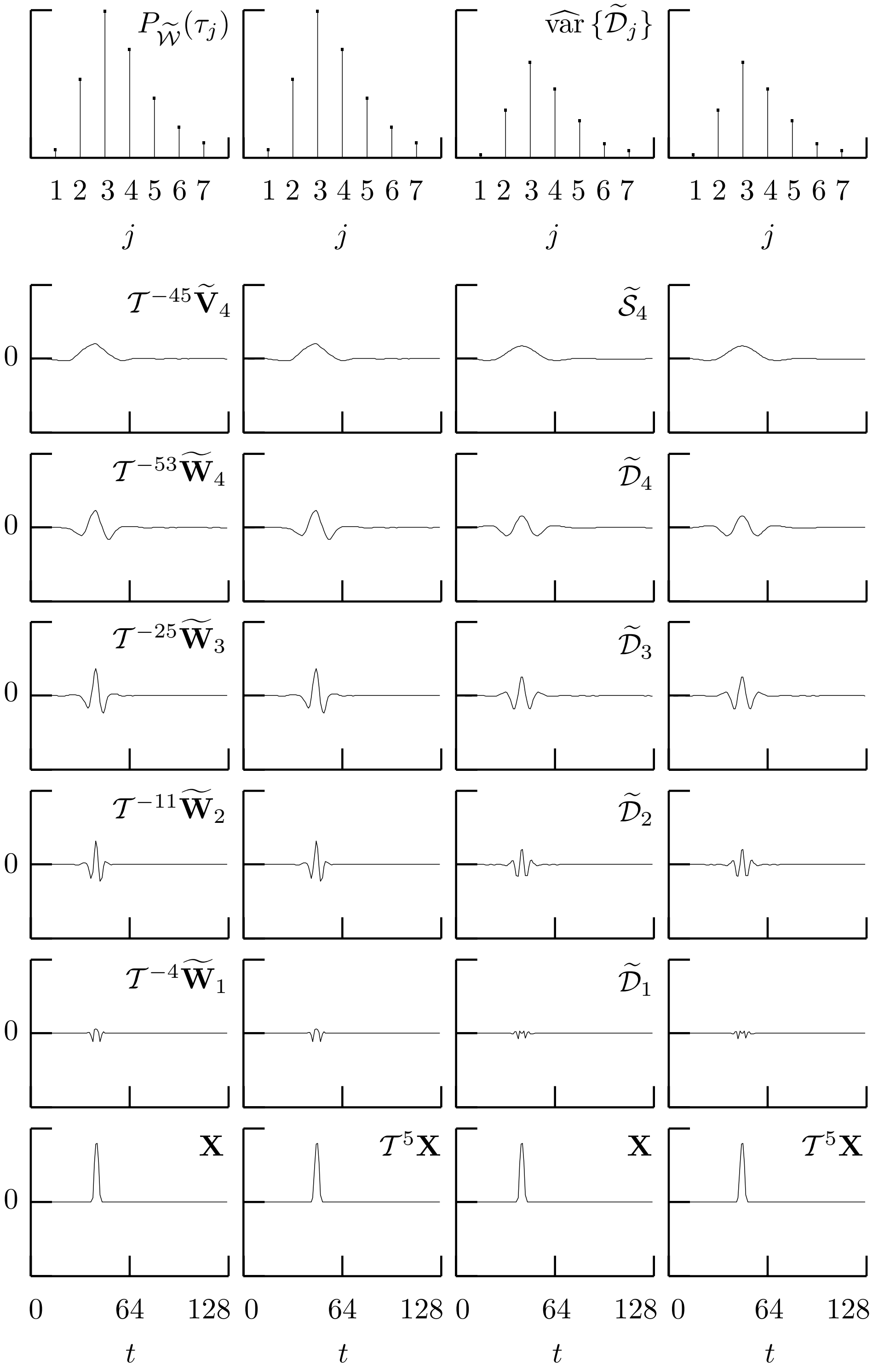

Figure 181. Bottom six rows as in Figure 161, with MODWT replacing DWT. The top row shows the discrete wavelet empirical power spectra (first two columns) and a corresponding quantity based upon level $j = 1, \ldots, 7$ MODWT details (last two columns) – see text for details.

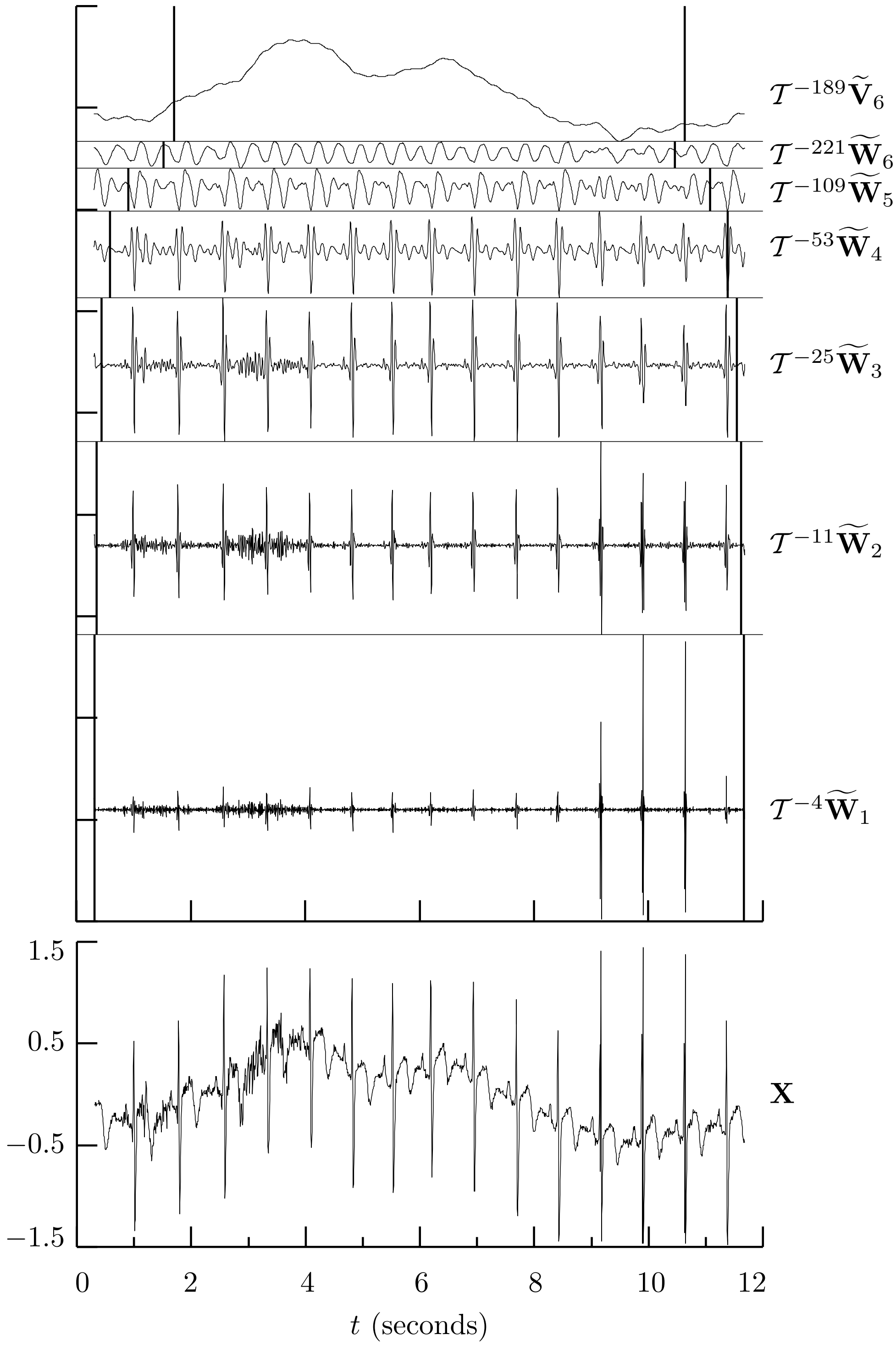

Figure 183. MODWT wavelet analysis of ECG time series using LA(8) wavelet. The above should be compared to Figure 127 for the corresponding DWT analysis (see text for details).

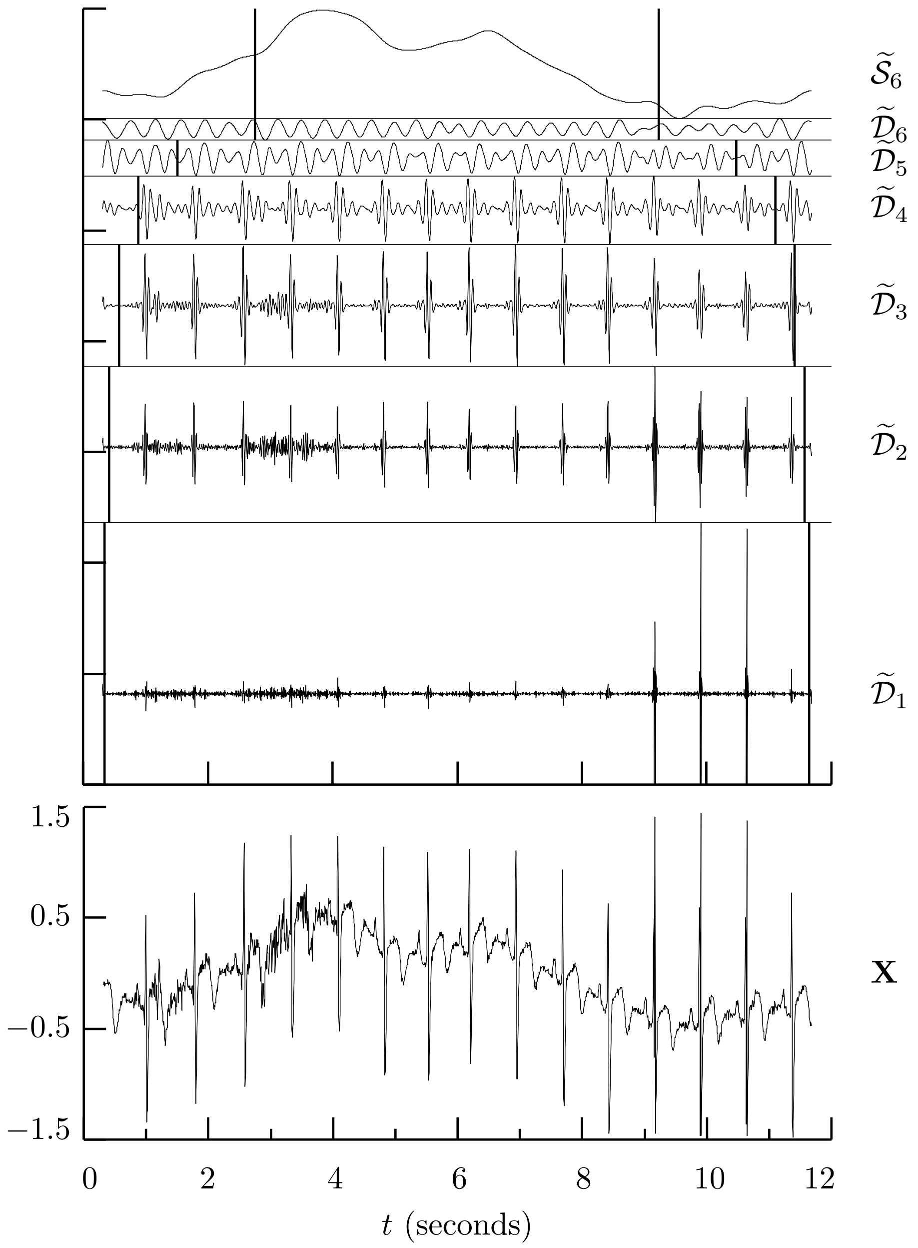

Figure 184. MODWT multiresolution analysis of ECG time series using LA(8) wavelet (see text for details). Figure 133 shows the corresponding DWT analysis.

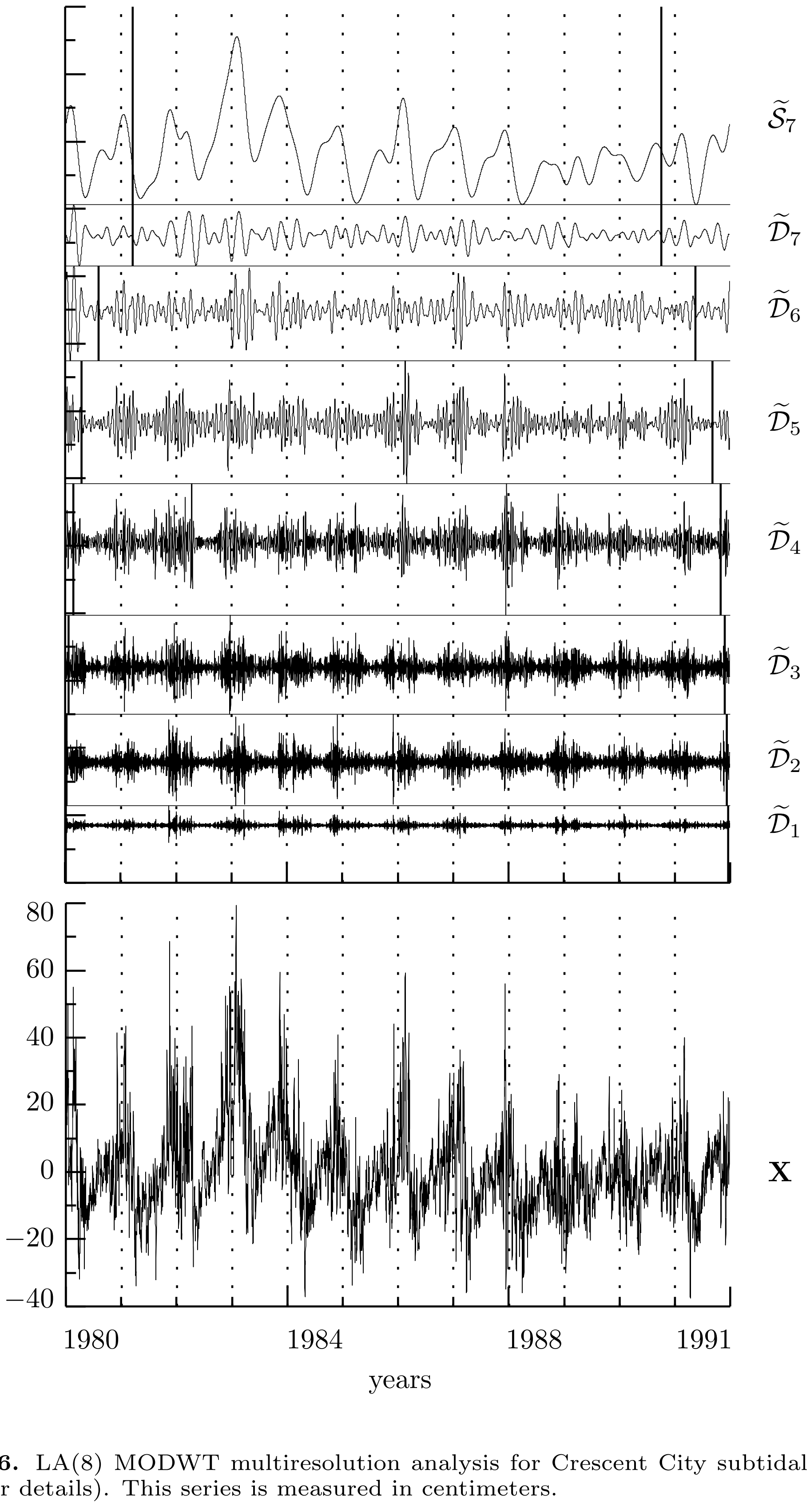

Figure 186. LA(8) MODWT multiresolution analysis for Crescent City subtidal variations (see text for details). This series is measured in centimeters.

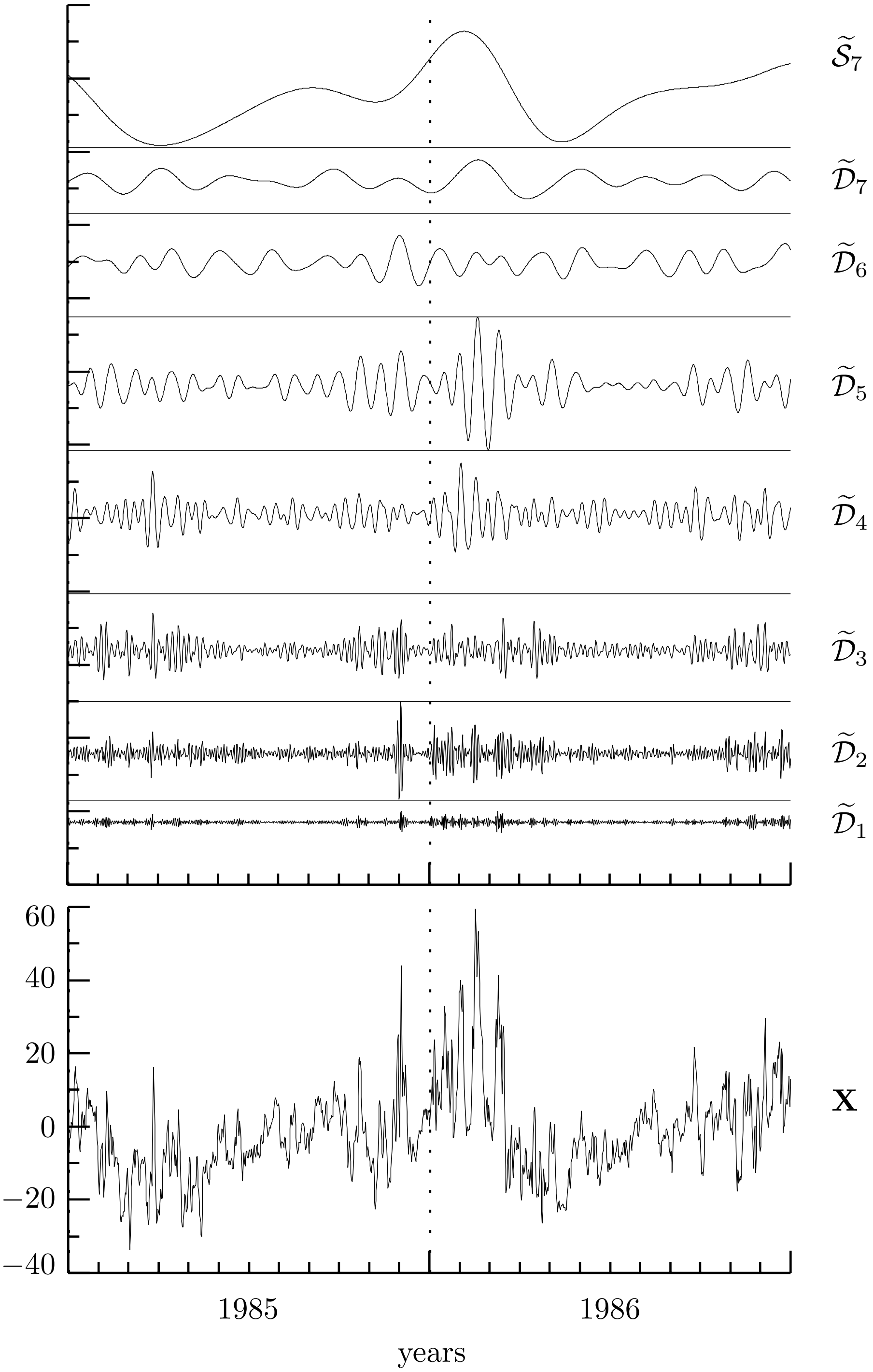

Figure 187. Expanded view of 1985 and 1986 portion of Figure 186.

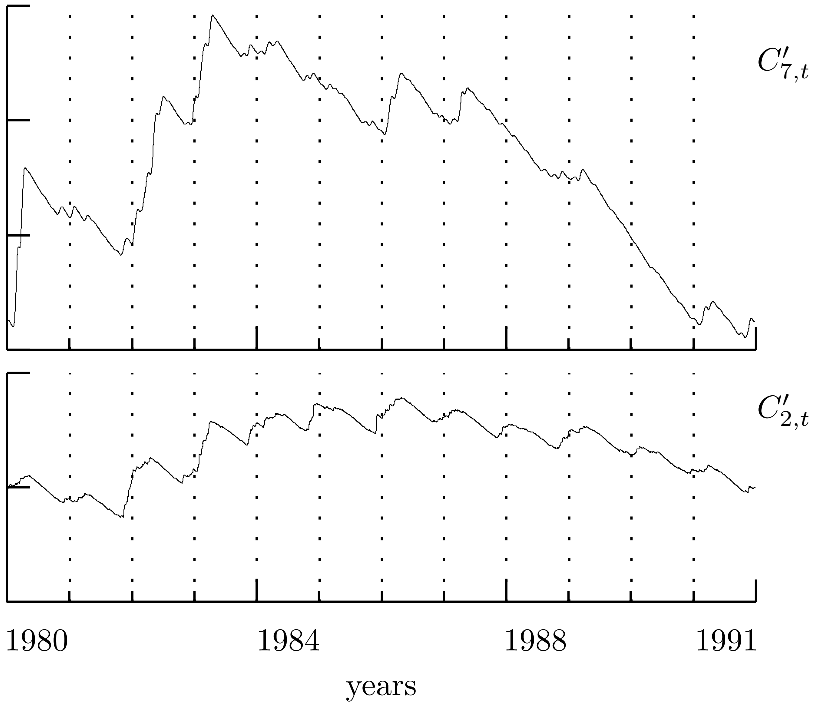

Figure 190. Rotated cumulative variance plots for subtidal sea level variations at physical scales $\tau_2\,\Delta t = 1$ day (bottom plot) and $\tau_7\,\Delta t = 32$ days (top).

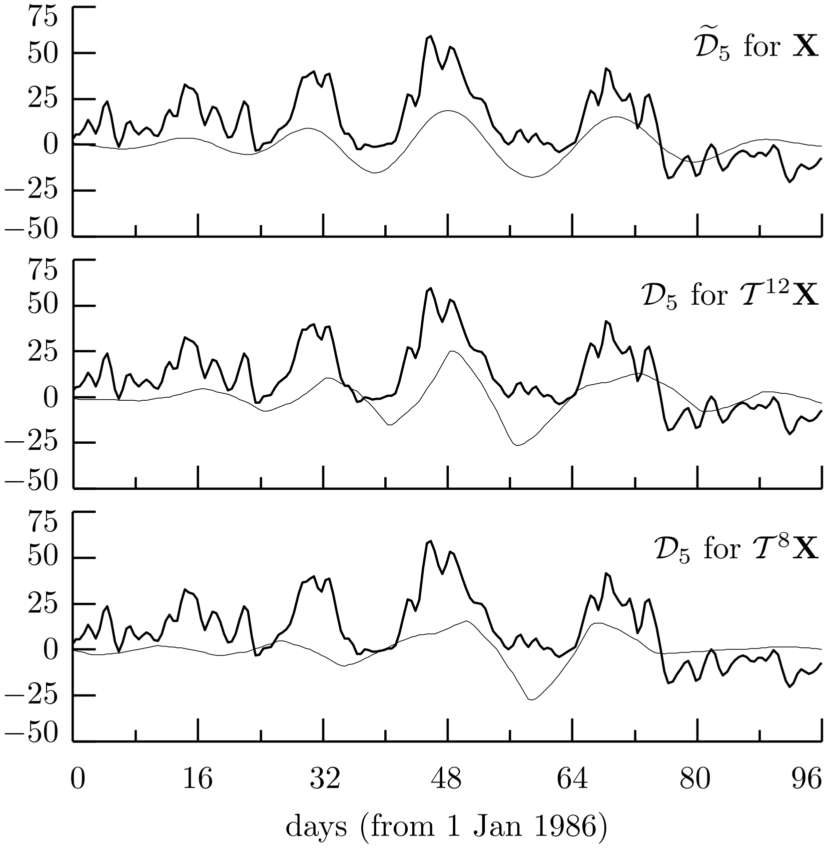

Figure 191. Demonstration of zero phase property of MODWT details. The thick curve in each plot is a 96 day portion of the Crescent City series starting at the beginning of 1986. The thin curves (from top to bottom) are the LA(8) MODWT detail $\widetilde{\mathcal{D}}_5$ for the original time series $\mathbf{X}$, the LA(8) DWT detail $\mathcal{D}_5$ for $\mathcal{T}^{12}\mathbf{X}$ (the time series delayed 12 data values) and the LA(8) DWT detail $\mathcal{D}_5$ for $\mathcal{T}^{8}\mathbf{X}$ (the time series delayed 8 data values). The physical scale associated with these details is $\tau_5\,\Delta t = 8$ days; i.e., the details should be associated with changes of averages on a scale of 8 days (this is the distance between minor tick marks on the horizontal axis).

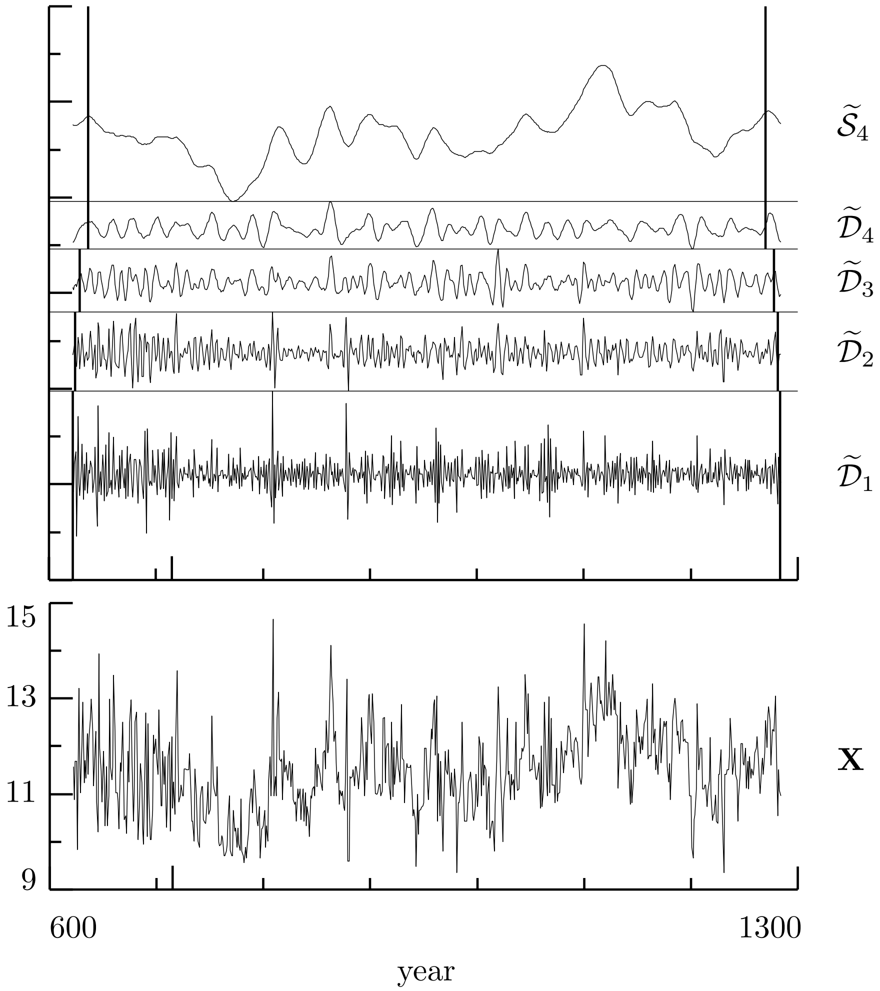

Figure 192. Level $J_0 = 4$ MODWT multiresolution analysis of Nile River minima (in meters) using the Haar wavelet filter.

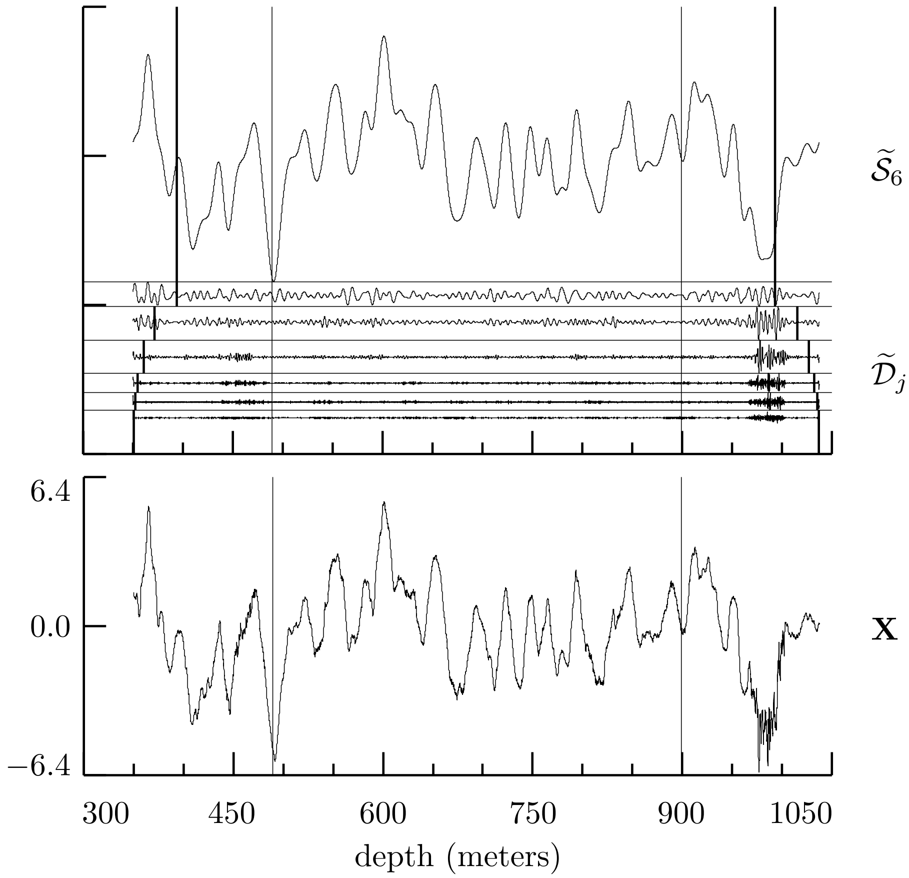

Figure 194. Level $J_0 = 6$ MODWT multiresolution analysis using LA(8) wavelet of vertical shear measurements (in inverse seconds) versus depth (in meters). This series was collected and supplied by Mike Gregg, Applied Physics Laboratory, University of Washington.

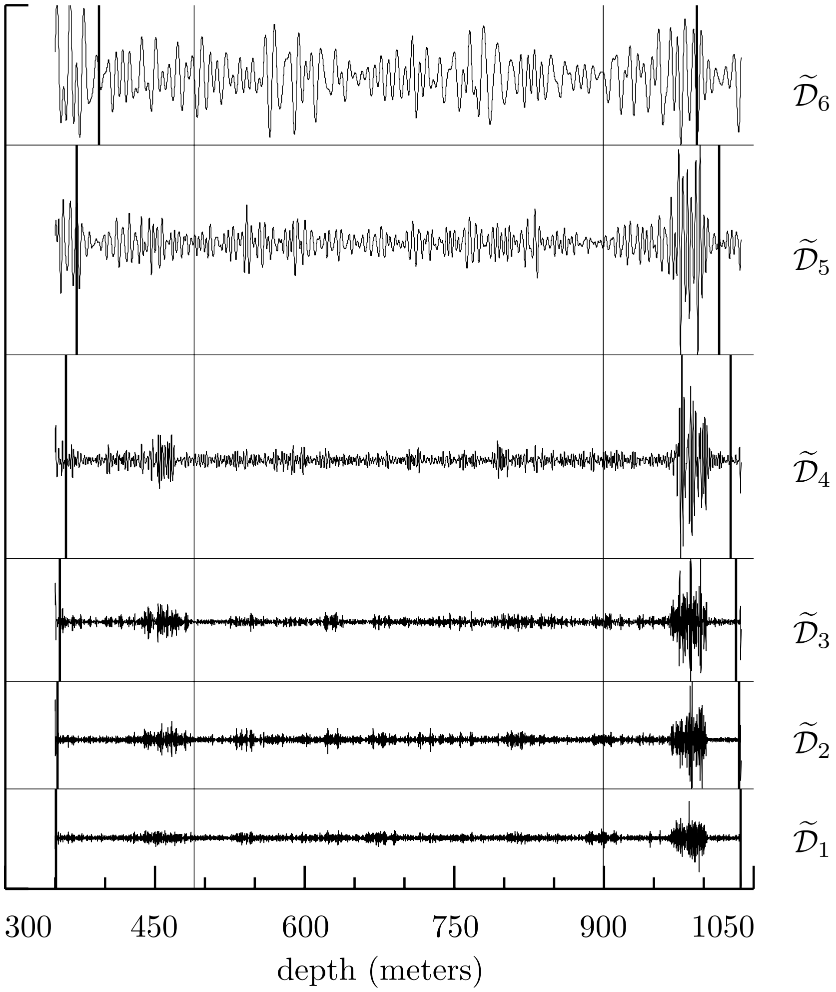

Figure 195. Expanded view of details series in MRA shown in Figure 194.

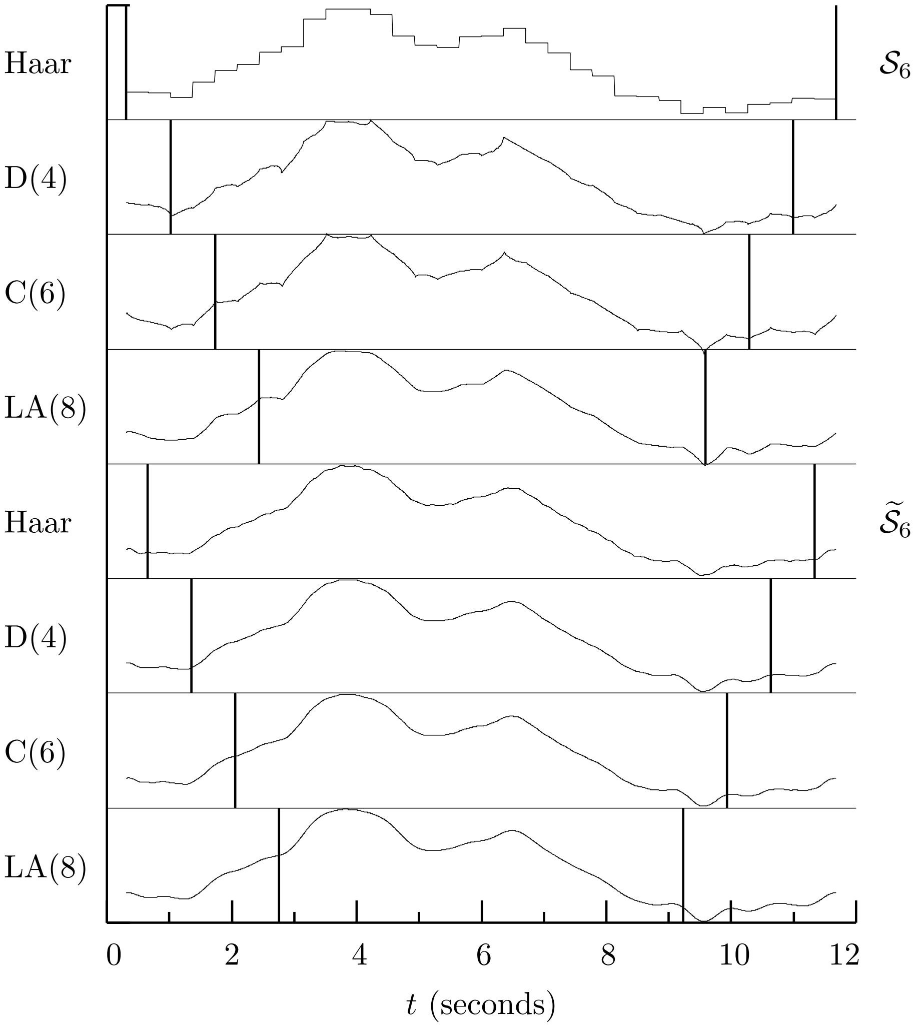

Figure 196. Comparison of DWT smooths $\mathcal{S}_6$ (top four series) and MODWT smooths $\widetilde{\mathcal{S}}_6$ (bottom four) for the ECG time series using, from top to bottom within each group, the Haar, D(4), C(6) and LA(8) wavelet filters. The thick vertical lines mark the boundary regions of the smooths, i.e., the parts of the smooths that are influenced (at least to some degree) by the assumption of circularity.

$\tilde{h}_l \equiv h_l/\sqrt{2}$	$\tilde{g}_l \equiv g_l/\sqrt{2}$
$\{\tilde{h}_l\} \longleftrightarrow \widetilde{H}(\cdot) = \frac{1}{\sqrt{2}} H(\cdot)$	$\{\tilde{g}_l\} \longleftrightarrow \widetilde{G}(\cdot) = \frac{1}{\sqrt{2}} G(\cdot)$
$\tilde{h}_l = (-1)^l \tilde{g}_{L-1-l}$	$\tilde{g}_l \equiv (-1)^{l+1} \tilde{h}_{L-1-l}$
$\widetilde{H}(f) = -e^{-i2\pi f(L-1)} \widetilde{G}(\frac{1}{2} - f)$	$\widetilde{G}(f) = e^{-i2\pi f(L-1)} \widetilde{H}(\frac{1}{2} - f)$
$\sum_l \tilde{h}_l = \widetilde{H}(0) \equiv 0$	$\sum_l \tilde{g}_l = \widetilde{G}(0) = 1$
$\sum_l \tilde{h}_l^2 \equiv \frac{1}{2}$	$\sum_l \tilde{g}_l^2 = \frac{1}{2}$
$\sum_l \tilde{h}_l \tilde{h}_{l+2n} \equiv 0, n \neq 0$	$\sum_l \tilde{g}_l \tilde{g}_{l+2n} = 0, n \neq 0$
$\sum_l \tilde{g}_l \tilde{h}_{l+2n} = 0$	
$\widetilde{\mathcal{H}}(f) \equiv \lvert\widetilde{H}(f)\rvert^2 = \frac{1}{2}\mathcal{H}(f)$	$\widetilde{\mathcal{G}}(f) \equiv \lvert\widetilde{G}(f)\rvert^2 = \frac{1}{2}\mathcal{G}(f)$
$\widetilde{\mathcal{H}}(f) + \widetilde{\mathcal{H}}(f + \frac{1}{2}) = 1$	$\widetilde{\mathcal{G}}(f) + \widetilde{\mathcal{G}}(f + \frac{1}{2}) = 1$
$\widetilde{\mathcal{G}}(f) + \widetilde{\mathcal{H}}(f) = 1$	
$\widetilde{W}_{1,t} \equiv \sum_l \tilde{h}_l X_{t-l \bmod N}$	$\widetilde{V}_{1,t} \equiv \sum_l \tilde{g}_l X_{t-l \bmod N}$
$\widetilde{W}_{j,t} = \sum_l \tilde{h}_l \widetilde{V}_{j-1,t-2^{j-1}l \bmod N}$	$\widetilde{V}_{j,t} = \sum_l \tilde{g}_l \widetilde{V}_{j-1,t-2^{j-1}l \bmod N}$
$\tilde{h}_{1,l} \equiv \tilde{h}_l,\ \ \widetilde{H}_1(f) \equiv \widetilde{H}(f)$	$\tilde{g}_{1,l} \equiv \tilde{g}_l,\ \ \widetilde{G}_1(f) \equiv \widetilde{G}(f)$
$\widetilde{H}_j(f) \equiv \widetilde{H}(2^{j-1}f) \prod_{l=0}^{j-2} \widetilde{G}(2^l f)$	$\widetilde{G}_j(f) \equiv \prod_{l=0}^{j-1} \widetilde{G}(2^l f)$
$\widetilde{H}_j(f) = \frac{1}{2^{j/2}} H_j(f)$	$\widetilde{G}_j(f) = \frac{1}{2^{j/2}} G_j(f)$
$\widetilde{H}_j(f) = \widetilde{H}(2^{j-1}f)\widetilde{G}_{j-1}(f)$	$\widetilde{G}_j(f) = \widetilde{G}(2^{j-1}f)\widetilde{G}_{j-1}(f)$
$\{\tilde{h}_{j,l}\} \longleftrightarrow \widetilde{H}_j(\cdot)$	$\{\tilde{g}_{j,l}\} \longleftrightarrow \widetilde{G}_j(\cdot)$
$\sum_l \tilde{h}_{j,l} = \widetilde{H}_j(0) = 0$	$\sum_l \tilde{g}_{j,l} = \widetilde{G}_j(0) = 1$
$\sum_l \tilde{h}_{j,l}^2 = \frac{1}{2^j}$	$\sum_l \tilde{g}_{j,l}^2 = \frac{1}{2^j}$
$\sum_l \tilde{h}_{j,l} \tilde{h}_{j,l+2^j n} = 0, n \neq 0$	$\sum_l \tilde{g}_{j,l} \tilde{g}_{j,l+2^j n} = 0, n \neq 0$
$\sum_l \tilde{g}_{j,l} \tilde{h}_{j,l+2^j n} = 0$	
$\widetilde{\mathcal{H}}_j(f) \equiv \lvert\widetilde{H}_j(f)\rvert^2 = \frac{1}{2^j}\mathcal{H}_j(f)$	$\widetilde{\mathcal{G}}_j(f) \equiv \lvert\widetilde{G}_j(f)\rvert^2 = \frac{1}{2^j}\mathcal{G}_j(f)$
$\widetilde{W}_{j,t} \equiv \sum_l \tilde{h}_{j,l} X_{t-l \bmod N}$	$\widetilde{V}_{j,t} \equiv \sum_l \tilde{g}_{j,l} X_{t-l \bmod N}$

Table 202. Key relationships involving MODWT wavelet and scaling filters (the conventions in Table 154 for limits on sums over l apply here too).